

Computationally efficient trajectory design from motion primitives for near time-optimal transitions for systems with oscillating internal dynamics.

1st Thomas Auer
IACE - UMIT TIROL
Hall in Tirol, Austria
thomas.auer@umit-tirol.at

2nd Frank Woittennek
IACE - UMIT TIROL
Hall in Tirol, Austria
frank.woittennek@umit-tirol.at

Abstract—An efficient approach to compute near time-optimal trajectories for linear kinematic systems with oscillatory internal dynamics is presented. Thereby, kinematic constraints with respect to velocity, acceleration and jerk are taken into account. The trajectories are composed of several motion primitives, the most crucial of which is termed jerk segment. Within this contribution, the focus is put on the composition of the overall trajectories, assuming the required motion primitives to be readily available. Since the scheme considered is not time-optimal, even decreasing particular constraints can reduce the overall transition time, which is analysed in detail. This observation implies that replanning of the underlying jerk segments is required as an integral part of the motion planning scheme, further insight into which has been analysed in a complementary contribution. Although the proposed scheme is not time-optimal, it allows for significantly shorter transition times than established methods, such as zero-vibration shaping, while requiring significantly lower computational power than a fully time-optimal scheme.

Note to Practitioners—This paper deals with trajectory planning for systems where oscillations at the end of the motion must be avoided, such as in high-precision pick-and-place processes. This paper presents a method of assembling trajectories from pre-planned motion profiles that is easy to implement. The method presented offers shorter transition times than existing and established methods such as trajectory shaping, allowing for increased throughput. As the overall reduction in transition time depends on the system and its parameters, a specific numerical example is provided. A supplementary publication provides a numerically efficient algorithm to compute the motion profiles for the system presented here. It is important to note, however, that other motion profiles can also be used, allowing this method to be applied to different systems. The requirements that these motion profiles must satisfy are given in this publication.

Index Terms—Motion-planning, Optimization methods, Motion Control

I. INTRODUCTION

Pick-and-place processes in the electrical industry demand accuracy and speed. Trends in the electronics industry point to miniaturisation and further integration of circuits from year to

This work has been submitted to the IEEE for possible publication. Copyright may be transferred without notice, after which this version may no longer be accessible.

year [16]. High accuracy is required for proper part placement to ensure electrical connections work as intended. In order to decrease cost, short transitions are desirable. Forces due to motion acting on the machine frame in combination with finite stiffness lead to oscillation and inaccuracy in component placement. The oscillation amplitudes of the machine frame can be bigger, than the allowed accuracy requirements, which are in the μm range [1]. Specifically planned motion profiles, also called trajectories, are used to achieve rest-to-rest transitions for the system.

A. Previous research in this topic

The so called S-Curve [8] is the fastest time optimal trajectory, that is limited in jerk, acceleration and velocity for rest-to-rest transitions of ideally stiff systems. Since production machines exhibit flexibility originating from the finite stiffness of the machine frame, it is usually not feasible to use the S-Curve directly, since it leads to oscillation. A method to plan rest-to-rest trajectories for systems exhibiting flexibility is the application of shaping techniques to those trajectories. This is commonly referred to as trajectory shaping. A common shaper, that is used for this purpose is the zero-vibration (ZV)-shaper [27]. A key advantage of trajectory shapers lies in its ease of implementation and the robustness w.r.t. to parameter uncertainty [20]. The sensitivity to parameter uncertainty of the ZV-shaper can be further reduced by increasing the system damping [25]. Further and more substantial improvements can be achieved by utilizing ZVD-shapers [18], [14], [13] or EI-shapers [26], [24], [32]. A very detailed overview concerning the shaping methods can be found in [29]. Decreasing the sensitivity to parameter uncertainty has been studied extensively, because it is an important topic. However, if the parameters of the system are known with a certain accuracy, methods offering shorter transition times can be of greater interest. A method to decrease transition times, when using trajectory shapers is to employ negative-impulse shapers [28]. However, even if the original trajectory does not violate any kinematic constraints, due to the nature of negative-impulse shapers, violations of kinematic constraints can occur for the shaped trajectory. While there are strategies to avoid violation

of kinematic constraints [30] and negative-impulse shapers allow for faster transitions, they are limiting the shape of the underlying trajectory and might still lack time-optimality in order to avoid violation of the kinematic constraints. Methods to adjust the underlying S-Curve trajectories in order to remove as much oscillation as possible have been studied in [17], [15]. By adjusting the maximal jerk and the duration, considerable amounts of oscillation can be removed without utilizing trajectory shapers. Those approaches share the property, that the damping of the system can not be taken into account, even if it is known. This leads to residual oscillation, even for the nominal model (no parameter uncertainty).

Employing feedback control concepts is a further possibility to improve the oscillation behaviour [6], [21], [22]. This allows to use fast shapers or trajectories planned without shapers and the insensitivity to parameter uncertainty can be ensured by the active control concept [9]. Approaches with feedback still benefit from fast trajectories that offer rest-to-rest transitions for the nominal model. In this case, the controller reduces the oscillation at the end of a transition. A disadvantage is, that additional measurement equipment might be required. Using trajectories planned to achieve oscillation free rest-to-rest transitions is still beneficial. Trajectories planned with optimal-control approaches guarantee the fastest transitions while respecting the kinematic constraints. Different planning methods including two optimal-control concepts were compared in [5]. Calculation through optimization of truly time-optimal trajectories can cause issues due to the discontinuous nature of the input signals required [23]. Implementation of the required numeric algorithms on programmable logic controllers (PLC) can be especially problematic due their limited computing power. Another issue that prevents such approaches from being used in actual pick-and-place machines consists in the lack of guarantees concerning the convergence of the underlying algorithms. A method to plan the motion out of trajectory segments, where each segment has to satisfy a number of constraints has been proposed in [10]. This method offers a time-advantage over a ZV-shaped trajectory at the expense of more complicated calculation, however the calculation effort required can be prohibitive, when it comes to using it on industrial machinery.

B. Contribution of this paper to the field

This publication explains, how to assemble the trajectories from certain motion primitives called jerk segments. The calculation of those segments has been separated into a distinct publication [3]. Within this contribution, the method to plan the trajectories is called OCP-J. In order to allow for small transition distances, the proposed algorithm permits the overlap of individual segments. It is shown, that lowering the limit for the acceleration can lead to faster overall rest-to-rest transitions. For the use-case this method was developed for, it is shown, that this method delivers time-optimal trajectory segments for the transitions between acceleration bounds. While further improvements in individual steps are still possible, this method allows faster transitions than the

existing ZV-shaper. It also offers better parameter stability, than the time-optimal solution and the efficient method of calculation allows for the calculation of trajectories in real time. The algorithm in this contribution is further designed in a way, that allows for overlapping of the trajectory segments, allowing for faster overall transitions and very small transition distances. Adaption to systems with multiple eigenfrequencies would further be possible, by switching out the jerk segments with different ones, that take multiple frequencies into account.

C. Organisation of paper

This section is organized into the following chapters. The mathematical model, the parameters and the most important mathematical background is introduced in Section II. Afterwards, the calculation of the full trajectory with the three different cases is explained in Section III. Formulating an overlying optimization problem to ensure the minimal transition times with the OCP-J approach is described in Section IV and the algorithms required are also summarised there. This section demonstrates, why it can be advantageous in some cases, if the calculation of the jerk segments can be completed quickly, which is the content of [3]. A comparison with regular full discretization and a ZV filter with regards to transition time and parameter sensitivity is shown in Section V. The results are then summarized in Section VI and points for relevant follow-up research are provided in Section VII.

II. PRELIMINARIES

A. Mathematical model

A pick-and-place machine exhibiting flexibility could be modelled using a continuum mechanic description, if every effect of the oscillation should be captured in detail. However, since the essential oscillation of the machine frame can be captured by the first mode, a simplified system description with a lumped model has been chosen. This model consists of two masses, a spring and a viscous damping element and is shown schematically in Figure 1. While this is a rather simple system, it is sufficient in modelling the motion and the focus of the contribution can be put on the effective method of calculation of the trajectory. The spring k represents the stiffness of the machine frame and the viscous damping element d the natural damping of the machine frame. The masses are the mass of the baseframe m_b and the mass of the slider m_s . In an actual production machine this slider would mount a gripper for component handling and it is commonly referred to as endeffector. The equations governing the motion

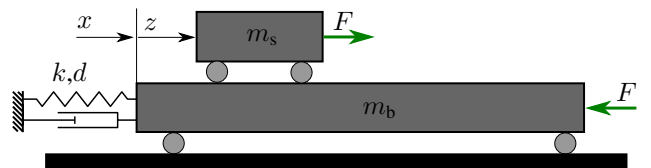


Fig. 1: Symbolic representation of one axis of the pick-and-place machine.

of the system [5, cf.] can be derived via momentum balance and are given by

$$m_b \ddot{x}(t) + d \dot{x}(t) + k x(t) = -F(t), \quad (1a)$$

$$m_s (\ddot{x}(t) + \ddot{z}(t)) = F(t), \quad (1b)$$

whereas any effects arising from friction are included in the force $F(t)$. Using a position controller for the slider position $z(t)$ on the actual production machines removes the influence of those forces by basically using $\ddot{z}(t)$ as input. The parameters used for the simulation studies in this contribution are listed in Table I. The kinematic constraints listed in Table II correspond

TABLE I: Parameters and resulting eigenfrequencies

$m_s = 25 \text{ kg}$	$m_b = 500 \text{ kg}$	$k = 15 \cdot 10^6 \text{ N/m}$	$d = 5 \cdot 10^3 \text{ kg/s}$
$f_0 = 26.9 \text{ Hz}$		$f_d = 26.8914 \text{ Hz}$	

to an exemplary production machine. It is advantageous to use

TABLE II: Kinematic constraints of slider.

$ \dot{z}(t) \leq v_{\text{lim}}$	$ \ddot{z}(t) \leq a_{\text{lim}}$	$ z^{(3)}(t) \leq j_{\text{lim}}$
$v_{\text{lim}} = 1.5 \text{ m/s}$	$a_{\text{lim}} = 20 \text{ m/s}^2$	$j_{\text{lim}} = 800 \text{ m/s}^3$

a dynamic extension with $z^{(3)}(t)$ as input for the calculations required later on. Adding (1a) and (1b) together to remove $F(t)$ and using $m_g = m_s + m_b$ leads to the state-space representation

$$\dot{\mathbf{x}} = \begin{bmatrix} 0 & 1 & 0 & 0 & 0 \\ -k^* & -d^* & 0 & 0 & -m^* \\ 0 & 0 & 0 & 1 & 0 \\ 0 & 0 & 0 & 0 & 1 \\ 0 & 0 & 0 & 0 & 0 \end{bmatrix} \cdot \begin{bmatrix} x \\ \dot{x} \\ z \\ \dot{z} \\ \ddot{z} \end{bmatrix} + \begin{bmatrix} 0 \\ 0 \\ 0 \\ 0 \\ 1 \end{bmatrix} z^{(3)} \quad (2)$$

$k^* = k/m_g \quad d^* = d/m_g \quad m^* = m_s/m_g$

with the state \mathbf{x} and input u given by

$$\mathbf{x} = [x, \dot{x}, z, \dot{z}, \ddot{z}]^T, \quad u = z^{(3)}. \quad (3)$$

If z is understood as the output of the system it can be readily observed that the system possesses relative degree 3 and is given in Byrnes-Isidori form. The internal dynamics, which obviously is not observable over this output corresponds to a damped harmonic oscillator with undamped eigenfrequency $\omega_0 = \sqrt{k^*}$ and damping ratio $\frac{d^*}{2\omega_0}$, which is excited by the slider acceleration \ddot{z} .

B. Solution of the slider dynamics

Twice continuously differentiable trajectories $t \mapsto z(t)$ are considered, which are piecewise constant in the input $u(t) = z^{(3)}(t)$. As a consequence, the jerk $z^{(3)}(t)$ is a sum of n steps of amplitudes a_1, \dots, a_n occurring at $t_1 < \dots < t_n$:

$$z^{(3)}(t) = \sum_{i=1}^n a_i H(t - t_i). \quad (4)$$

Therein, $H(\cdot)$ represents the Heaviside step function. The terminal time of the trajectory motion is denoted by $t_{f,t}$. Integration of (4) leads to

$$\ddot{z}(t) = \ddot{z}(0) + \sum_{i=1}^n a_i H(t - t_i) \cdot (t - t_i), \quad (5a)$$

$$\dot{z}(t) = \dot{z}(0) + \ddot{z}(0)t + \frac{1}{2} \sum_{i=1}^n a_i H(t - t_i) \cdot (t - t_i)^2, \quad (5b)$$

$$z(t) = z(0) + \dot{z}(0)t + \ddot{z}(0)\frac{t^2}{2} + \frac{1}{6} \sum_{i=1}^n a_i H(t - t_i) \cdot (t - t_i)^3. \quad (5c)$$

As the considered trajectories should correspond to rest-to-rest transitions of the slider, they must satisfy¹

$$z^{(3)}(0) = 0, \quad \ddot{z}(0) = 0, \quad \dot{z}(0) = 0, \quad (6a)$$

$$z^{(3)}(t_{f,t}) = 0, \quad \ddot{z}(t_{f,t}) = 0, \quad \dot{z}(t_{f,t}) = 0. \quad (6b)$$

Evaluating the initial and final conditions (6) in view of (4) and (5) yields the following relations for the coefficients in (4):

$$\sum_{i=1}^n a_i = 0, \quad \sum_{i=1}^n a_i t_i = 0, \quad \sum_{i=1}^n a_i t_i^2 = 0.$$

An example for such a trajectory is the so-called S-Curve [8] which is also used as reference trajectory in ZV and ZVD-shaping as shown in Figure 2.

C. Optimal control formulation

For a general time-invariant non-linear system with state-space description

$$\dot{\mathbf{x}} = \mathbf{f}(\mathbf{x}(t), \mathbf{u}(t)), \quad \mathbf{x}(t) \in \mathbb{R}^n, \mathbf{u}(t) \in \mathbb{R}^m \quad (7)$$

an optimal control problem aims to compute the minimum

$$\min_{\mathbf{x}, \mathbf{u}, t_{f,t}} J(\mathbf{x}, \mathbf{u}, t_{f,t}), \quad (8a)$$

of a cost functional

$$J(\cdot) = V(\mathbf{x}(t_{f,t}), t_{f,t}) + \int_0^{t_{f,t}} \ell(\mathbf{x}(t), \mathbf{u}(t), t) dt, \quad (8b)$$

involving the Lagrangian ℓ and the Mayer term V (cf. [2], [12] for details). Thereby, for $t \in [0, t_{f,t}]$ the variables \mathbf{x} and \mathbf{u} are constrained by the state-space equation (7) and

$$\mathbf{u}(t) \in \mathcal{U}, \quad \mathbf{x}(t) \in \mathcal{X}, \quad \mathbf{x}(0) \in \mathcal{X}_0, \quad \mathbf{x}(t_{f,t}) \in \mathcal{X}_f.$$

Start- and terminal-conditions of the state are taken into account by $\mathcal{X}_0 \subset \mathbb{R}^n$ and $\mathcal{X}_f \subset \mathbb{R}^n$ respectively. The state is constrained to the subset $\mathcal{X} \subset \mathbb{R}^n$ and the input to $\mathcal{U} \subset \mathbb{R}^m$.

¹Formally, the condition $z^{(3)}(t_{f,t}) = 0$ is not really required in the formulation of the corresponding optimal control problem. However, it can always be satisfied by choosing $t_n = t_{f,t}$ with an appropriate choice of a_n , leaving $t \rightarrow z^{(i)}(t)$, $i = 0, 1, 2$ unchanged on $[0, t_{f,t}]$. In fact, it ensures $\ddot{z}(t) = \dot{z}(t) = 0$ not only at $t = t_{f,t}$ but for all $t \geq t_{f,t}$, i.e., the system remains in the desired equilibrium. Moreover, the formulation chosen essentially simplifies the algebraic computations.

The main objective of contribution consists in computing time-optimal trajectories or at least nearly time-optimal rest-to-rest trajectories for the system (2). The corresponding optimal control problem [4] is obtained by using the terminal time of the transition $t_{f,t}$ directly as cost

$$J(\cdot) = t_{f,t},$$

which corresponds to the choice $\ell(\mathbf{x}(t), \mathbf{u}(t), t) = 1$ and $V(\mathbf{x}(t_{f,t}), t_{f,t}) = 0$ in (8b). Moreover, (7) is replaced by (3), and the initial and terminal constraints are given by

$$\begin{aligned} \mathbf{x}(0) &= [0, 0, 0, 0, 0]^T, \\ \mathbf{x}(t_{f,t}) &= [0, 0, z_f, 0, 0]^T \end{aligned}$$

with $z_f = z(t_{f,t})$ being the target point for the transition $t_{f,t}$. As a consequence, the complete system including the internal dynamics is at rest at the end of the slider transition as long as u is chosen according to $u(t) = z^{(3)}(t) = 0$, $t \geq t_{f,t}$. The state variables concerning the slider motion $\dot{z}(t)$ and $\ddot{z}(t)$ as well as the input $z^{(3)}(t)$ are constrained according to the limits given in Table II. The trajectory presented in Figure 2 has been calculated using a full discretization approach [19], [11], [7], [31], [4] to solve this optimization problem. If the optimization problem is formulated for the entire transition and solved in one step, the method is called OCP-S in this contribution. An exemplary trajectory is shown in Figure 2 and it is compared to the S-Curve trajectory [8] and a trajectory calculated with a ZV-shaper [27]. The transition distance of 300 mm shown can be considered a large distance in the context of the pick-and-place machines considered. The S-Curve represents the

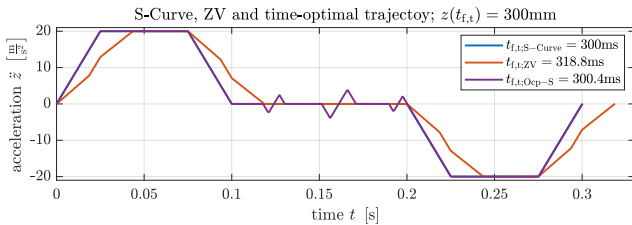


Fig. 2: Trajectories: S-Curve, ZV and OCP-S for a comparison of transition times for the motion distance $z(t_{f,t}) = 300$ mm.

fastest transition from a start-point to an end-point, while respecting the kinematic constraints from Table II. However, the excitation of the internal dynamics of the system leads to oscillation and as a result to a loss of accuracy. ZV-shaping is a common method to achieve rest-to-rest transitions. The two main drawbacks of OCP-S are the effort for computing the trajectory (calculation time) and the sensitivity to parameter uncertainties [5]. For this reason [5] included a comparison to a method called OCP-J. In OCP-J, the trajectory for the full transition is assembled from preplanned motion primitives. A comparison to existing trajectory planning methods is shown in Section V (Figure 15 in Section V expands the comparison shown in Figure 2 to also include the OCP-J trajectory) and in greater detail also in [5]. This contribution explains the

algorithms and mathematical background used for this second method (OCP-J) in detail and highlights the advantages.

III. METHOD EXPLAINED: OCP-J

This section provides an overview over OCP-J. Rather than solving an optimization problem for the full trajectory like OCP-S, the OCP-J method assembles trajectories from motion primitives, some of them are the solution of smaller optimization problems. The proposed method is strongly inspired by the standard S-Curve (cf. [8]). However, in contrast to the latter, which constitutes the time-optimal trajectory when neglecting the internal dynamics in (2), OCP-J does not result in an exact solution of the optimal-control problem (8a).

For fixed kinematic constraints and given plant parameters, the particular sequence of motion primitives depends on the terminal position z_f . Exemplary trajectories planned with this method are shown in Figure 3. The trajectory on

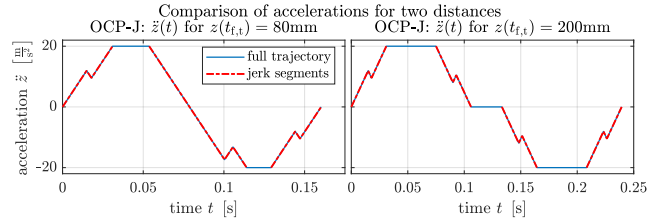


Fig. 3: Two OCP-J trajectories illustrating the method (picture taken from [5]).

the left represents a rather short transition distance, where only the maximum acceleration a_{lim} is reached, but not the maximum velocity v_{lim} . In contrast, the trajectory on the right corresponds to a larger distance, where both a_{lim} and v_{lim} are reached. In both trajectories the segments coloured in red are crucial. These motion primitives are called jerk segments in this work and planned in such a way, that the internal dynamics is at rest at the start and the end of those segments. This results in an optimization problem similar to the one introduced in the previous section. The initial conditions and terminal constraints at the free end time $t = t_f$ are given by

$$\ddot{x}(0) = -k^*x(0) - m^*\ddot{z}(0) = 0, \quad \dot{x}(0) = 0 \quad (10a)$$

$$\ddot{x}(t_f) = -k^*x(t_f) - m^*\ddot{z}(t_f) = 0, \quad \dot{x}(t_f) = 0. \quad (10b)$$

Moreover, within this contribution the following initial and terminal constraints for the acceleration segments are considered

$$\ddot{z}(t_f), \ddot{z}(0) \in \{-a_{max}, 0, a_{max}\}, \quad \ddot{z}(0) \neq \ddot{z}(t_f).$$

Moreover, the terminal velocity and terminal position are unconstrained while initial values $z(0)$ and $\dot{z}(0)$ may be specified. Above, the maximal acceleration a_{max} does not necessarily coincide with² a_{lim} .

²Note that, due to the particular construction of the trajectories it can be beneficial to choose $a_{max} < a_{lim}$ where a_{lim} is the limit according to the specification. This is emphasized in Subsection III-E.

By choosing the duration the slider moves at constant acceleration (resp. velocity) appropriately, the total transition distance can be adjusted (cf. Figure 3). Within this contribution several cases requiring different calculations for trajectory planning are considered. Their dependence on the final position z_f is illustrated in Figure 4 and characterized as follows:

- **Case 1:** A trajectory, where a_{\max} is reached, but v_{\lim} is not reached and there is only one jerk segment to get from a_{\max} to $-a_{\max}$.
- **Case 2:** A trajectory, where a_{\max} and v_{\lim} are reached.
- **Case 3:** A trajectory, where a_{\max} is reached and v_{\lim} is not reached. This case exists for distances to large for Case 1, but to small for Case 2. It is rare and only required for certain distances as shown in Figure 4. This special case is considered in Subsection III-D.

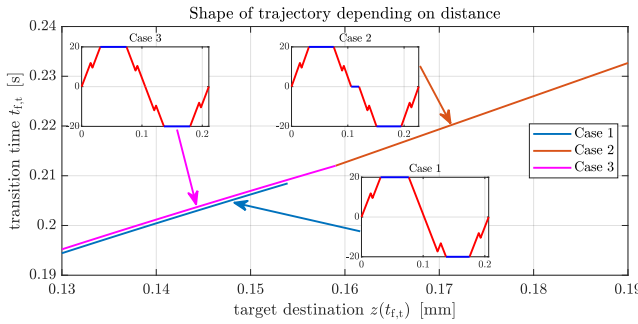


Fig. 4: Trajectories for multiple distances and regions associated with different cases.

A. Preprocessing of jerk segments

As Algorithm 2 describes, after calculating the jerk segments for the given a_{\max} , the velocity differences ($v_{f1, f2, f3}$) and some travel distances ($s_{f1, f2, f3}$) for the segments themselves have to be calculated. Those values are required when computing the full trajectories. The jerk segments and the corresponding parameters are highlighted in Figure 5 as a part of a particular trajectory. Although this trajectory corresponds to Case 1, the parameters computed also apply the remaining cases. The jerk $z^{(3)}(t)$ of the jerk segments is piece-wise constant, as depicted in Figure 3 and shown in [3]. As a consequence, it can be written in the form (4). Therefore, the corresponding velocity and the position result from (5).

Following this procedure, the parameters s_{f1} and v_{f1} , associated with the first jerk segment, are given by

$$s_{f1} = z(t_{f1}), \quad v_{f1} = \dot{z}(t_{f1}),$$

where $t \mapsto z(t)$ and t_{f1} can be computed by minimizing t_{f1} subject to the given kinematic constraints and the system dynamics (2). The latter is complemented by the initial and final conditions, given by (10) and

$$z(0) = 0, \quad \dot{z}(0) = 0, \quad \ddot{z}(0) = 0, \quad \ddot{z}(t_{f1}) = a_{\max}.$$

Moreover, $s_{f2} = z(t_{f2})$, $v_{f2} = \dot{z}(t_{f2})$ are obtained in the same way for initial and terminal conditions

$$z(0) = 0, \quad \dot{z}(0) = 0, \quad \ddot{z}(0) = a_{\max}, \quad \ddot{z}(t_{f2}) = -a_{\max}.$$

Finally, t_{f3} , $s_{f3} = z(t_{f3})$, and $v_{f3} = -\dot{z}(t_{f3})$ follow from the boundary conditions

$$z(0) = 0, \quad \dot{z}(0) = 0, \quad \ddot{z}(0) = -a_{\max}, \quad \ddot{z}(t_{f2}) = 0.$$

B. Case 1

The general shape of the solution is shown in Figure 5. In order to reach the desired final position with the slider, the jerk segments have to be connected by segments with constant acceleration. In particular, acceleration $\ddot{z}(t)$ remains at a_{\max} during the intervals $[T_1, T_2]$ of duration t_1 and at $-a_{\max}$ during the interval $[T_3, T_4]$ of duration t_2 as shown in Figure 5. To compute the durations t_1 and t_2 , the precomputed

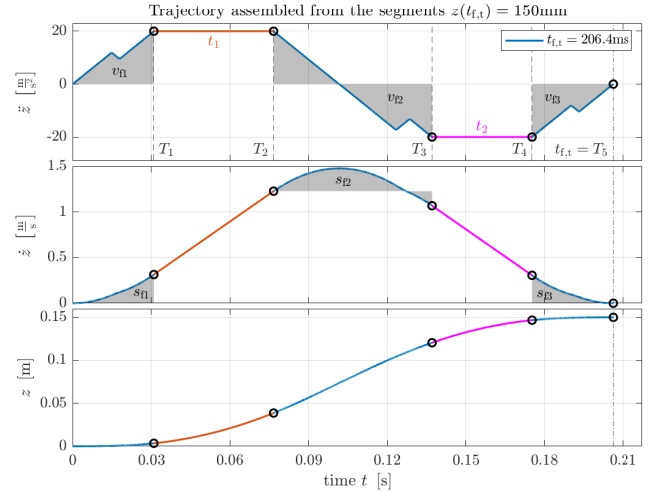


Fig. 5: OCP-J trajectory for Case 1.

values $s_{f1, f2, f3}$ and $v_{f1, f2, f3}$, as explained in Subsection III-A, are employed. As mentioned previously, the times $t_{f1, f2, f3}$ are the terminal times of the individual jerk segments and they satisfy

$$t_{f1} = T_1, \quad t_{f2} = T_3 - T_2, \quad t_{f3} = t_{f1} = T_5 - T_4.$$

The velocities at the concatenation points T_1, \dots, T_5 can be derived to be

$$\begin{aligned} v(T_1) &= v_{f1}, \\ v(T_2) &= v_{f1} + t_1 \cdot a_{\max}, \\ v(T_3) &= v_{f1} + t_1 \cdot a_{\max} + v_{f2}, \\ v(T_4) &= v_{f1} + t_1 \cdot a_{\max} + v_{f2} - t_2 \cdot a_{\max}, \\ v(T_5) &= v_{f1} + t_1 \cdot a_{\max} + v_{f2} - t_2 \cdot a_{\max} - v_{f3}. \end{aligned} \quad (12a)$$

Moreover, the respective positions are given by

$$\begin{aligned}
s(T_1) &= s_{f1} , \\
s(T_2) &= s_{f1} + \int_0^{t_1} v(\tau) d\tau = s_{f1} + t_1 \cdot v_{f1} + \frac{1}{2} a_{\max} \cdot t_1^2 , \\
s(T_3) &= s(T_2) + (v_{f1} + t_1 \cdot a_{\max}) \cdot t_{f2} + s_{f2} , \\
s(T_4) &= s(T_3) + (v_{f1} + t_1 \cdot a_{\max} + v_{f2}) \cdot t_2 - \frac{1}{2} a_{\max} \cdot t_2^2 , \\
s(T_5) &= s(T_4) + s_{f3} = z(t_{f,t}) .
\end{aligned}$$

Therefore, using $s_f = s_{f1} + s_{f2} + s_{f3}$, the final position is:

$$\begin{aligned}
z(t_{f,t}) &= s_f + v_{f1} t_{f2} + t_1(v_{f1} + a_{\max}(t_{f2} + t_2)) + \dots \\
&\quad t_1^2 \frac{a_{\max}}{2} + t_2(v_{f1} + v_{f2}) - t_2^2 \frac{a_{\max}}{2} . \quad (14)
\end{aligned}$$

From (12a) and $v(T_5) = 0$, it follows, that

$$v(T_5) = 0 = v_{f1} + t_1 \cdot a_{\max} + v_{f2} - t_2 \cdot a_{\max} - v_{f3} . \quad (15)$$

Solving (15) for t_2 and inserting into (14) leads to

$$0 = t_1^2 + p \cdot t_1 + q$$

with

$$\begin{aligned}
p &= \frac{a_{\max} t_{f2} + 2 v_{f1} + v_{f2}}{a_{\max}} , \\
q &= -\frac{z(t_{f,t})}{a_{\max}} + \frac{s_{f1} + s_{f2} + s_{f3} + v_{f1} t_{f2}}{a_{\max}} + \dots \\
&\quad \frac{(v_{f1} + v_{f2} + v_{f3}) \cdot (v_{f1} + v_{f2} - v_{f3})}{2 a_{\max}^2} .
\end{aligned}$$

This allows to solve for t_1 directly. From the two possible solutions for t_1 , the smaller one, which is always negative, is ignored. Therefore, the time t_1 is calculated with:

$$t_1 = -\frac{p}{2} + \sqrt{\frac{p^2}{4} - q} . \quad (17)$$

For small transition distances q may be negative which results in negative values for t_1 . This leads to overlapping jerk segments, which, however, can be a viable solution. A detailed discussion of this case, which is illustrated in Figure 8 and Figure 9, can be found in Subsection III-E. Having computed t_1 , the duration t_2 follows immediately from (15). The resulting trajectory is checked and it is calculated, if one of the other cases (Case 2 or Case 3) would be the actual solution. This is explained in further detail in Algorithm 2 in Subsection IV-C.

C. Case 2

This case has to be considered, if the kinematic velocity constraint would be violated in Case 1 (see Algorithm 2 in Subsection IV-C). The general shape of the solution is shown in Figure 6. It consists of overall seven individual segments, and can be divided into an acceleration phase on the interval $[0, T_3]$, followed by a constant velocity phase on $[T_3, T_4]$ with duration $t_{v-\max} = T_4 - T_3$, and, finally, a deceleration phase on $[T_4, T_7]$. Therein the acceleration phase is composed of three segments, a jerk segment on the interval $[0, T_1]$, a segment

of constant acceleration on $[T_1, T_2]$ and another jerk segment on $[T_2, T_3]$. Similarly, the deceleration phase consists of a jerk segment on the interval $[T_4, T_5]$, a segment of constant acceleration on $[T_5, T_6]$ and another jerk segment on $[T_6, T_7]$.

First, the time at maximal acceleration a_{\max} to reach v_{\lim} results from

$$v_{\lim} = v_{f1} + v_{f3} + a_{\max} t_{a-\max} ,$$

with the abbreviation $t_{a-\max} = T_2 - T_1 = T_6 - T_5$ and the velocity differences v_{f1} and v_{f3} according to Subsection III-A. This yields

$$t_{a-\max} = \frac{v_{\lim} - (v_{f1} + v_{f3})}{a_{\max}} . \quad (18)$$

Note that high acceleration limits a_{\max} may imply $v_{f1} + v_{f3} > v_{\lim}$ which would result in $t_{a-\max} < 0$ and, therefore, intersecting segments, i.e., $T_2 < T_1$. This is discussed later in this section (cf. also Figure 9 in Subsection III-E). From the considerations in Subsection III-A the symmetry

$$\ddot{z}(t + T_4) = -\ddot{z}(t) , \quad t \in [0, T_3]$$

can be deduced, which, together with $\dot{z}(T_4) = v_{\lim}$, implies

$$\dot{z}(t + T_4) = v_{\lim} - \dot{z}(t) \quad (19a)$$

$$z(t + T_4) = z(T_4) + t v_{\lim} - z(t) , \quad t \in [0, T_3] . \quad (19b)$$

Denote by $s_{\text{acc}} = z(T_3)$ and $s_{\text{dec}} = z(T_4 + T_3) - z(T_4)$ the total distances travelled during the acceleration and deceleration phases, respectively. According to (19b) these distances satisfy

$$s_{\text{acc}} + s_{\text{dec}} = v_{\lim} T_3 = v_{\lim} \cdot (2 \cdot t_{f1} + t_{a-\max}) .$$

For the sake illustration, this relation and the underlying symmetries (19) have been visualized in Figure 6. As a consequence of the above, the final position $z(t_{f,t})$ reached is given by

$$z(t_{f,t}) = v_{\lim} t_{v-\max} + v_{\lim} \cdot (2 \cdot t_{f1} + t_{a-\max}) .$$

Therefore, for a given target position, the time spent at maximum velocity v_{\lim} reads

$$t_{v-\max} = \frac{z(t_{f,t}) - v_{\lim} \cdot (2 \cdot t_{f1} + t_{a-\max})}{v_{\lim}} . \quad (20)$$

D. Case 3

There are certain situations (travelling distances) where neither Case 1 nor Case 2 applies. For these distances the velocity constraint is violated on the interval $[T_2, T_3]$ when using Case 1. For the same distances the maximal velocity is not reached when using Case 2 which results in $t_{v-\lim} < 0$. The particular travelling distances (for the parameter set and kinematic constraints used in this publication) corresponding to this situation are shown in Figure 4.

In the described situation Case 3 is used for trajectory design. The general shape of the trajectory for this case is shown in Figure 7. It consists of overall six individual segments, and can be divided into an acceleration phase on the

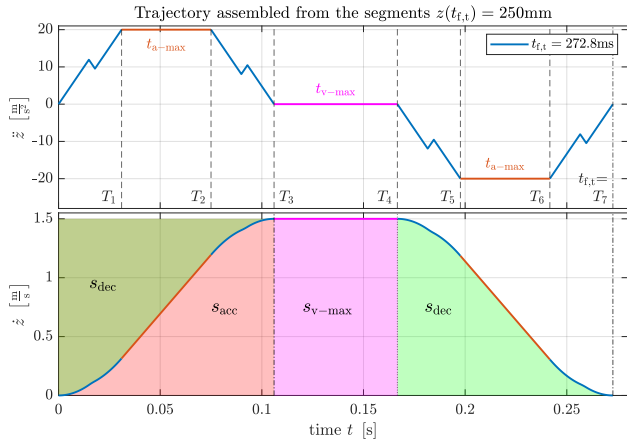


Fig. 6: OCP-J trajectory for Case 2.

interval $[0, T_3]$, directly followed by the deceleration phase on $[T_4, T_7]$, whereas $T_3 = T_4$. Similarly to Case 2 these phases are composed of two jerk segments connected by a constant-acceleration segment. In contrast to Case 2, maximum velocity v_{lim} does not need to be reached. Instead, the duration $T_2 - T_1 = T_6 - T_5 = t_{a-max}$ of the constant-acceleration segments are computed such that the final position $z(t_f)$ is reached (cf. Figure 7). As a prerequisite, the distances travelled

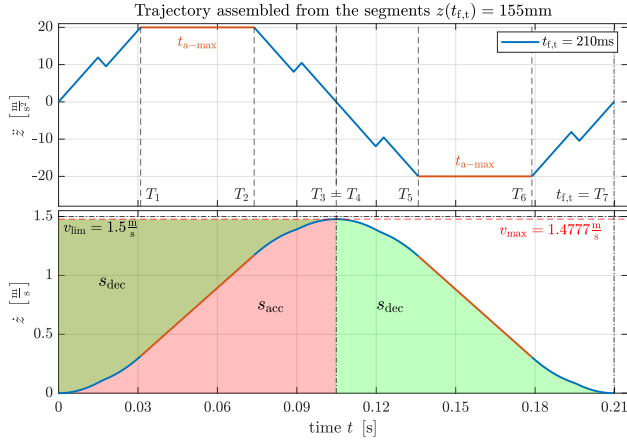


Fig. 7: OCP-J trajectory for Case 3.

during the acceleration and deceleration can be computed by employing the same symmetries as in Case 2 (cf. Figure 7). With $v_{max} = \dot{z}(T_3)$ the maximum velocity reached, this yields

$$\begin{aligned} z(t_{f,t}) &= v_{max} \cdot (2 \cdot t_{f1} + t_{a-max}) \\ &= (v_{f1} + v_{f3} + a_{max} t_{a-max}) \cdot (2 \cdot t_{f1} + t_{a-max}) . \end{aligned}$$

Using $v_f = v_{f1} + v_{f3}$ allows to rewrite

$$0 = t_{a-max}^2 + t_{a-max} \cdot \underbrace{\frac{2 a_{max} t_{f1} + v_f}{a_{max}}}_p + \underbrace{\frac{2 t_{f1} \cdot v_f - z(t_{f,t})}{a_{max}}}_q .$$

Determining t_{a-max} by choosing the positive branch of the square-root solution yields

$$t_{a-max} = -\frac{p}{2} + \sqrt{\frac{p^2}{4} - q} . \quad (22)$$

As in Case 1, $q > 0$ leading to $t_{a-max} < 0$ is not explicitly excluded.

E. Violation of jerk constraints

As discussed in Subsection III-B, Subsection III-C and Subsection III-D the jerk segments may intersect in certain situations and they are allowed to. However, for particular parameters this overlap may cause a violation of the jerk constraints as shown in Figure 8 and Figure 9. This subsection analyses these violations in more detail and shows how they can be avoided. A reduction of a_{max} is a possibility to avoid these

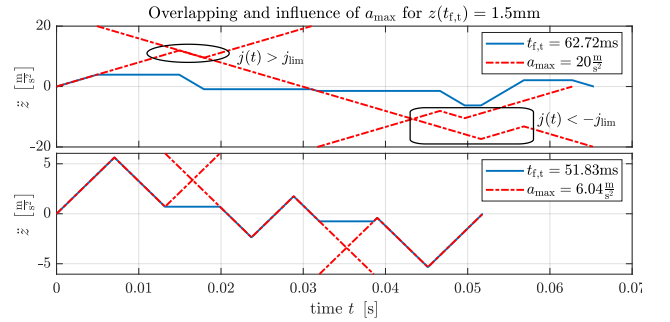


Fig. 8: Superposition of intersecting jerk segments in Case 1. Top: original maximum acceleration causes a violation of the jerk constraint. Bottom: Reduced maximum acceleration avoids violation of the jerk constraint and reduces $t_{f,t}$.

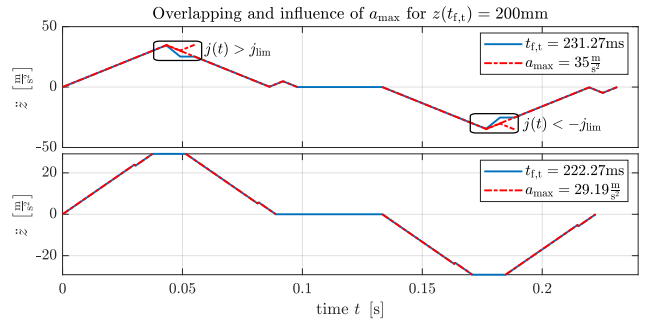


Fig. 9: Superposition of intersecting jerk segments in Case 2. Top: original maximum acceleration causes a violation of the jerk constraint. Bottom: Reduced maximum acceleration avoids violation of the jerk constraint and reduces $t_{f,t}$.

violations, as shown in Figure 8 and Figure 9. This is outlined in Algorithm 3. For the considered parameter set, a detailed analysis of the influence of the maximum acceleration a_{max} on the transition time and the violation of the jerk constraint is shown in Figure 10. Regions corresponding to a violation of the kinematic constraints are hatched. This overview suggests, that there is an optimal acceleration for each distance. When

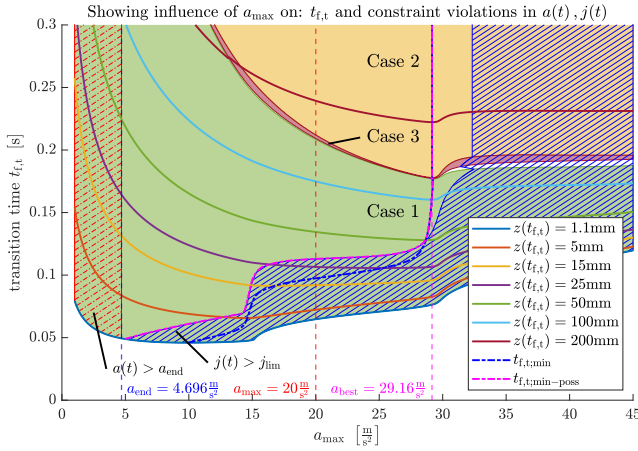


Fig. 10: Influence of a_{\max} on $t_{f,t}$.

using the proposed design method, it is advantageous to use the ideal acceleration instead of the highest possible acceleration. Since the optimal feasible acceleration a_{\max} depends on the travel distance, the calculation of the jerk segments has to be implemented in an efficient manner. An efficient algorithm for the solution of this optimal control problem is presented in [3]. As highlighted by Figure 10, there is a region where very low accelerations a_{\max} can lead to $a(t) > a_{\max}$ for the finished trajectory as shown in Figure 11. For the parameters

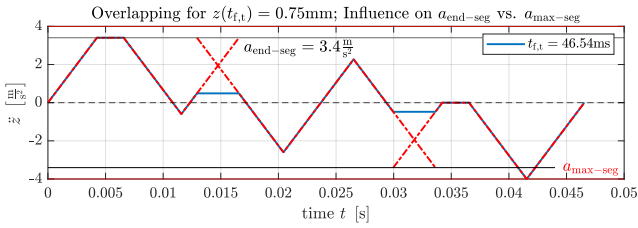


Fig. 11: Trajectory showing, that $a(t) < a_{\lim} = 20 \text{ m/s}^2$, even though $a(t) > a_{\max}$.

presented here, this only occurs for very low accelerations a_{\max} . In particular, for the example depicted in Figure 11, the constraint a_{\lim} is satisfied although \ddot{z} exceeds a_{\max} . A method to calculate the ideal acceleration for Case 2: $a_{\max} = a_{\text{best}}$ as marked in Figure 10 is outlined in Section IV.

IV. OPTIMIZING THE FULL TRAJECTORY

As mentioned in Subsection III-E and shown in Figure 10, adjustments of the maximal acceleration a_{\max} used for planning of the jerk segments can lead to an overall reduction of transition times. This motivates the higher-level optimization problem considered in this section. It is thereby assumed that for given maximal acceleration a_{\max} , the overall trajectory is calculated according to Section III. Based on that, the total transition time $t_{f,t}$ is optimized with respect to a_{\max} as the scalar optimization variable. The calculation is developed in detail for Case 2, while a detailed analysis of the remaining cases is postponed to future work.

A. Ideal acceleration a_{\max} for Case 2

The total transition time for the overall trajectory in Case 2 is

$$t_{f,t} = 4 \cdot t_{f1} + 2 \cdot t_{a-\max} + t_{v-\max}$$

with t_{f1} being the terminal time of a single jerk segment, $t_{a-\max}$ the time at maximum acceleration and deceleration and $t_{v-\max}$ the time at maximum slider velocity (see Figure 6). Using (18) and (20) leads to

$$t_{f,t}(a_{\max}) = \frac{z(t_{f,t})}{v_{\lim}} + \frac{v_{\lim}}{a_{\max}} + 2t_{f1}(a_{\max}) - \frac{v_{f1}(a_{\max}) + v_{f3}(a_{\max})}{a_{\max}}.$$

Searching for the optimal a_{\max} to minimize $t_{f,t}$ is a static optimization problem and the extrema (local minimum or maximum) satisfy

$$\frac{d}{da_{\max}} t_{f,t}(a_{\max}) = 0.$$

Differentiating $t_{f,t}(a_{\max})$ with regards to a_{\max} in order to minimize $t_{f,t}(a_{\max})$ gives

$$\frac{1}{a_{\max}^2} \left[2a_{\max}^2 \frac{d}{da_{\max}} t_{f1}(a_{\max}) + v_{f1}(a_{\max}) + v_{f3}(a_{\max}) - v_{\lim} - a_{\max} \cdot \frac{d}{da_{\max}} (v_{f1}(a_{\max}) + v_{f3}(a_{\max})) \right] = 0 \quad (23)$$

Solving (23) for a_{\max} gives the optimal acceleration a_{best} for Case 2. This confirms, that the optimal acceleration for Case 2 is independent of the transition distance as suggested by the results shown in Figure 10. However, as Case 2 can only be used on a certain interval of distances as shown in Figure 4, the optimal value for a_{\max} may still depend on the transition distance. The result for the derivation of $t_{f,t}(a_{\max})$ is plotted in Figure 12. The result shows, that there exists several local

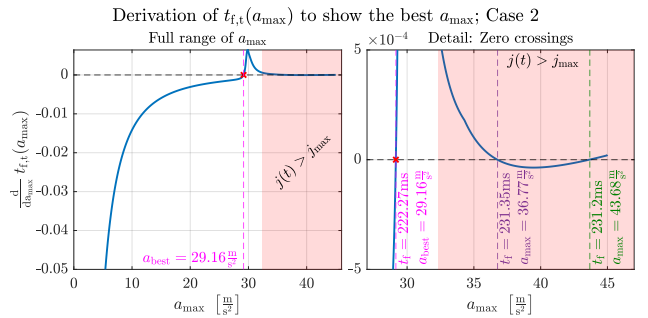


Fig. 12: Best acceleration for this set of parameters (Case 2).

optima, at least for the particular parameters used here.

B. Optimal maximum acceleration for Cases 1 and 3

In contrast to Case 2, the optimal a_{\max} for Cases 1 and 3 also depend on the overall transition distance, because of the terms $z(t_{f,t})/a_{\max}$ in (17) and (22) respectively. As Figure 10 suggests, the ideal acceleration for Case 1 and Case 3 can be slightly higher or lower than the ideal acceleration obtained for Case 2. This is underlined by Figure 13, which shows the results of a more detailed numerical analysis. Here the globally

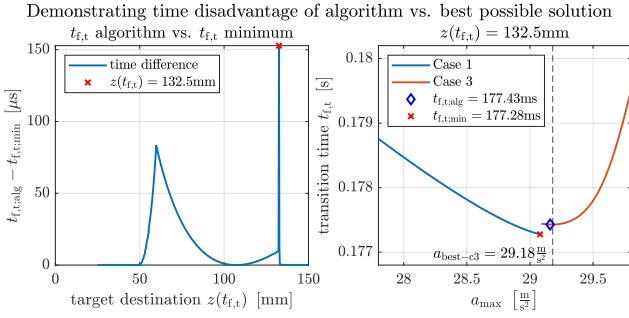


Fig. 13: Applying the algorithm to the trajectories and comparing the transition times with the best possible transition times to show the effectiveness of the algorithm (specific for distance).

optimal a_{\max} was evaluated and the transition time is compared to the transition time achieved with the algorithm described in Subsection IV-C. This result shows, that for a certain range of distances the result of the algorithms described below could be further improved. As the result in Figure 13 shows, the potential for improvement for the parameter set considered here is below $200\mu\text{s}$, which is smaller, than a single PLC cycle. For this reason, it was postponed for future work.

C. Algorithms required for calculation

This section contains the algorithms to calculate the full trajectories from the jerk segments and highlights the conditions used to select the different cases. It furthermore highlights necessary adjustments to a_{\max} , to ensure minimal transition times and to avoid violation of kinematic constraints. In order to calculate a full trajectory Algorithm 1 is used. The algo-

Algorithm 1 Get OCP-J total

- 1: Calculate a_{best} with (23) ▷ Only required once
 - 2: Limit a_{best} to a_{lim}
 - 3: Calculate OCP-J trajectory with Algorithm 2 for a_{best}
 - 4: **if** $a(t) \leq a_{\text{lim}}$ and $j(t) \leq j_{\text{lim}} \forall t \in [0, t_{f,t}]$ **then**
 - 5: **return** OCP-J trajectory
 - 6: **else**
 - 7: Run Algorithm 3
 - 8: **return** OCP-J trajectory
 - 9: **end if**
-

gorithm requires the calculation of an individual trajectory with Algorithm 2. If the kinematic constraints are not violated, the computed trajectory can be exported, otherwise Algorithm 3 has to be called. A search algorithm iterates over possible a_{\max} values and searches for the highest a_{\max} possible, where no kinematic constraint is violated. This can be achieved efficiently with a binary search as outlined in Algorithm 3. Defining suitable limits for $n_{\text{max-iter}}$ and $\Delta t_{\text{boundary}}$ ensures termination of the search algorithm after a given number of iterations. As a consequence, Algorithm 2 might be called multiple times from Algorithm 3, therefore requiring, that calculation is efficient and quick. The algorithm to calculate

Algorithm 2 Get OCP-J trajectory for a_{\max}

- 1: Get segment for a_{\max} ▷ Use [3]
 - 2: Get segment for $2 a_{\max}$ ▷ Use [3]
 - 3: Calculate s_{f1}, \dots, v_{f3}
 - 4: Calculate OCP-J trajectory for Case 1
 - 5: **if** $v(t) \leq v_{\text{lim}} \forall t \in [0, t_{f,t}]$ **then**
 - 6: **return** OCP-J trajectory for Case 1
 - 7: **else**
 - 8: **if** $s(t_f) \geq s_{f,\text{min-Case 2}}$ **then**
 - 9: Calculate OCP-J trajectory for Case 2
 - 10: **return** OCP-J trajectory for Case 2
 - 11: **else**
 - 12: Calculate OCP-J trajectory for Case 3
 - 13: **return** OCP-J trajectory for Case 3
 - 14: **end if**
 - 15: **end if**
-

Algorithm 3 Optimize a_{\max}

- 1: Initialize $\Delta a_{\text{ges}} = a_{\text{best}}$
 - 2: Set $n_{\text{iter}} = 1$
 - 3: Set $a_{\text{iter}} = \frac{1}{2} \Delta a_{\text{ges}}$
 - 4: **repeat**
 - 5: Get trajectory with Algorithm 2 for $a_{\max} = a_{\text{iter}}$
 - 6: $n_{\text{iter}} = n_{\text{iter}} + 1$
 - 7: **if** $a(t) \leq a_{\text{lim}}$ and $j(t) \leq j_{\text{lim}} \forall t \in [0, t_{f,t}]$ **then**
 - 8: Save $t_{f,t}$ and calculate $\Delta t_f = t_{f,t,(k-1)} - t_{f,t,k}$
 - 9: **if** $t_{f,t,k} < t_{f,t,\text{best}}$ **then**
 - 10: $t_{f,t,\text{best}} = t_{f,t,k}$
 - 11: Save trajectory for export
 - 12: **end if**
 - 13: Set $a_{\text{iter}} = a_{\text{iter}} + (\frac{1}{2})^{n_{\text{iter}}} \cdot \Delta a_{\text{ges}}$
 - 14: **else**
 - 15: Set $a_{\text{iter}} = a_{\text{iter}} - (\frac{1}{2})^{n_{\text{iter}}} \cdot \Delta a_{\text{ges}}$
 - 16: **end if**
 - 17: **until** $\Delta t_f \leq \Delta t_{\text{boundary}} \vee n_{\text{iter}} > n_{\text{max-iter}}$
 - 18: **return** Trajectory from step 11 of Alg.
-

the jerk segments in this fashion is explained in [3]. To demonstrate, how frequent adjustments to a_{\max} are, trajectories for different distances have been planned and the resulting optimal values for a_{\max} and the total calculation times are shown in Figure 14. This shows, that adjustments of a_{\max} are

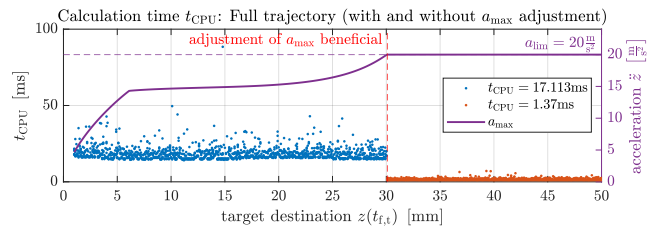


Fig. 14: Showing a_{\max} and t_{CPU} (average times over the points marked) used for different transition distances.

required only for small overall distances (below 30 mm for

the given parameters). Note that, working with precomputed jerk segments from prior runs is not always possible as the process parameters may change due to parameter drift. This is the reason, why the algorithm presented in [3], allowing efficient calculation of the jerk segments, is beneficial. The time measurements shown here were performed on a regular PC (not on a PLC) and are given only for reference.

V. COMPARISON WITH EXISTING METHODS

This section is devoted to a comparison with established trajectory planning methods like the S-Curve and ZV-shaping as well as to OCP-S. Repeating the calculation of the trajectories shown in Figure 2, but also adding the OCP-J approach shows, that a reduction of transition time could be achieved, when comparing to a ZV-shaped trajectory. This new comparison is shown in Figure 15. The transition time and parameter sensi-

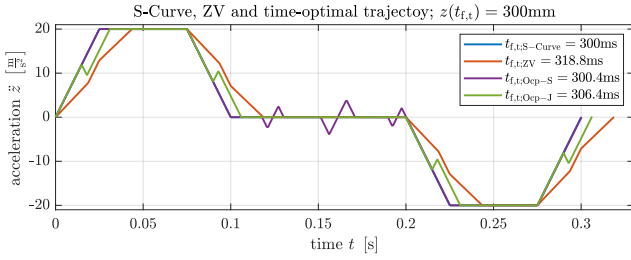


Fig. 15: Trajectories: S-Curve, ZV, OCP-S and OCP-J for a comparison of transition times for the motion distance $z(t_{f,t}) = 300$ mm.

tivity of different trajectory planning methods were analysed in detail in [5]. The transition times for all the methods for distances between 1 mm and 300 mm are shown in Figure 16 (plot taken from [5]). The parameter sensitivity was analysed

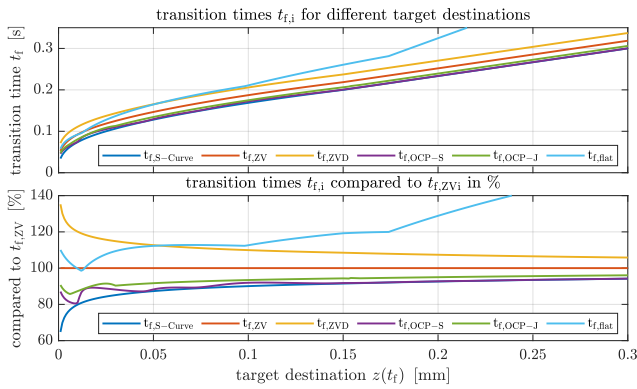


Fig. 16: Transition times for all methods. Shown are the absolute times and the times relative to the ZV-shaper. The comparison is made to the ZV-shaper, because it is the established method (plot taken from [5]).

in detail in [5] and is shown for +10% and -10% parameter variation in Figure 17 (plot taken from [5]).

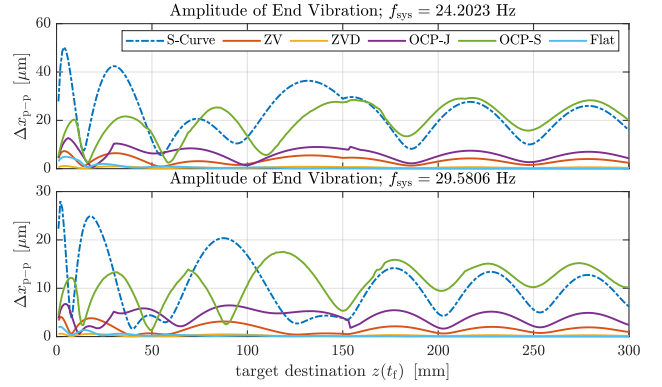


Fig. 17: Parameter sensitivity for the methods, that are being compared (plot taken from [5]).

Comparison to ZV and OCP-S

As shown in [25], higher damping leads to slightly higher insensitivity in the ZV-shaper. This is not the case for the OCP-J-approach as Figure 18 shows. This is best visible, when comparing the insensitivity curves (term introduced in [27]) for the different approaches. The term insensitivity curve refers

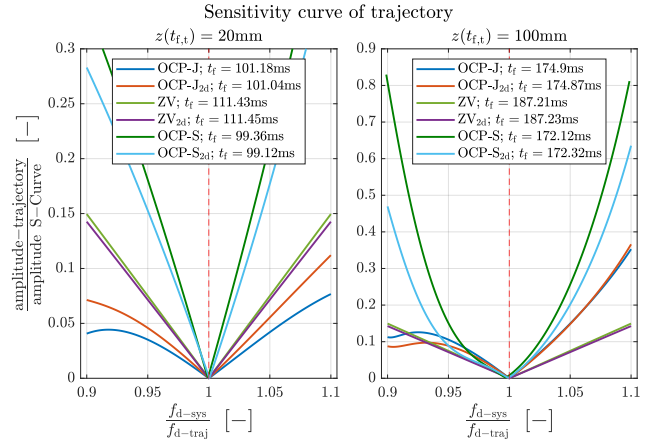


Fig. 18: Insensitivity curves: Comparison of a ZV-shaped S-Curve, the OCP-S trajectory and the OCP-J trajectory with different damping constants d .

to the ratio of residual oscillation amplitudes obtained for the trajectory planning method considered and the residual oscillation obtained for an S-Curve. The plot in Figure 18 shows the insensitivity curves of a ZV-shaped S-Curve and a OCP-J trajectory and the OCP-S trajectory. The first trajectories were planned with the parameters from Table I and the second trajectories with a damping constant d that is twice as high, than the one listed in Table I. Though the insensitivity curves do not show the absolute values of the respective amplitudes, two observations can be made. Firstly, the insensitivity curves for the OCP-J approach depend on the travel distance, while the ones for the ZV do not. Secondly, higher damping does not necessarily reduce sensitivity, when considering the OCP-J approach. Generally, the sensitivity to parameter uncertainties

is bigger, when using the OCP-J approach for most distances as Figure 17 shows. Despite this drawback, the main objective of reducing overall transition time at low and predictable computational cost compared to the OCP-S approach is achieved as well as lower overall sensitivity to parameter uncertainty (when comparing OCP-J to OCP-S).

VI. SUMMARY OF METHODS AND CONCLUSION

A novel way to calculate trajectories has been introduced. It was demonstrated, that recalculation of the segments can be beneficial, which prompted the development of the algorithm in [3] alongside this publication to perform the necessary calculations. This publication introduced the required algorithms, to be able to use those jerk segments to perform the necessary trajectory calculations. A comparison to established methods and to a method based on regular optimal trajectory planning demonstrates the potential with regard to transition time. While the parameter sensitivity is worse for some distances, when compared to the established ZV-shaper, there is still a significant improvement with comparison to the optimal control method OCP-S. While there is most likely some improvement potential left, when it comes to individual steps of the calculation, the presented approach overall offers a powerful method to calculate trajectories that realise a time-advantage. The calculation further does not rely on complicated optimization procedures or algorithms, which enables implementation on low powered PLC's.

VII. OUTLOOK

This section contains the outlook and conclusion. A few points for follow-up research were mentioned in the previous sections. Here they are summarized and additional points are provided. The most important next step is an implementation on a PLC to test the computation times on actual hardware. When doing this, the calculation times can be analysed with more accuracy. Adapting the algorithm to only allow switches of jerk on full controller cycles will be studied in the future as well in combination with active control algorithms on a production machine. Detailed analysis with regards to the algorithm employed to optimize a_{\max} might allow to solve for the actual best a_{best} for Case 1 and Case 3 as well. In this context, mathematically proving what the a_{best} is, could prove useful in further developing the algorithm. Since adaption to multiple eigenfrequencies requires to switch out the algorithm used to calculate the jerk segments (content of [3], but leave the calculations shown in here the same), studies on systems with multiple eigenfrequencies can be considered with the approach as well. Further analysis, if this algorithm can be extended to allow OCP-S trajectories to be calculated in a similar way, may provide even faster transition times and allow calculation on a PLC.

REFERENCES

- [1] Jonathan Abdilla, Uwe Bayer, Ruurd Boomsma, Stephan Bulcher, Alexander Kalss, Stephan Martin, Harald Meixner, Thiago Moura, Hubert Selhofer, Wolfgang Voegelé, and Martin Widauer. Thermo compression bonding for large dies under protective atmosphere. In *2020 IEEE 70th Electronic Components and Technology Conference (ECTC)*. IEEE, jun 2020.
- [2] Michael Athans and Peter L. Falb. *Optimal control - An Introduction to the Theory and Its Applications*. Dover Publ., Mineola, New York, 2007.
- [3] Thomas Auer and Frank Woittennek. Efficient calculation of time-optimal motion primitives for systems exhibiting oscillatory internal dynamics with multiple applications. *preprint*, 2024.
- [4] Thomas Auer, Phillip Kronthaler, and Frank Woittennek. Optimalsteuerungsentwurf für ein elastisch gekoppeltes Flächenportal mit Vergleich zu Standardverfahren. *7. IFToMM D-A-CH Konferenz*, 2021: 18./19. Februar 2021:Online-Konferenz, 2021.
- [5] Thomas Auer and Frank Woittennek. On trajectory design for flexible structures with input and state constraints. *IFAC*, 2023.
- [6] Dibakar Bandopadhyaya, Dileep Bhogadi, B. Bhattacharya, and A. Dutta. Active vibration suppression of a flexible link using ionic polymer metal composite. In *2006 IEEE Conference on Robotics, Automation and Mechatronics*. IEEE, December 2006.
- [7] John T. Betts. Survey of numerical methods for trajectory optimization. *Journal of Guidance, Control, and Dynamics*, 21(2):193–207, mar 1998.
- [8] Luigi Biagiotti Claudio Melchiorri. *Trajectory Planning for Automatic Machines and Robots*. Springer-Verlag GmbH, October 2008.
- [9] Avinash Gopal Dharne and Suhada Jayasuriya. Robust adaptive control of residual vibration in point-to-point motion of flexible bodies. *Journal of Vibration and Control*, 13(7):951–968, July 2007.
- [10] B.G. Dijkstra, N.J. Rambaratsingh, C. Scherer, O.H. Bosgra, M. Steinbuch, and S. Kerssemakers. Input design for optimal discrete time point-to-point motion of an industrial xy-positioning table. In *Proceedings of the 39th IEEE Conference on Decision and Control (Cat. No.00CH37187)*, CDC-00. IEEE, 2007.
- [11] C.R. Hargraves and S.W. Paris. Direct trajectory optimization using nonlinear programming and collocation. *Journal of Guidance, Control, and Dynamics*, 10(4):338–342, July 1987.
- [12] Leslie M. Hocking. *Optimal Control - An Introduction to the Theory with Applications*. Oxford University PressOxford, February 1991.
- [13] Chul-Goo Kang. Impulse vectors for input-shaping control: A mathematical tool to design and analyze input shapers. *IEEE Control Systems*, 39(4):40–55, aug 2019.
- [14] Mateusz Kasprowiak, Arkadiusz Parus, and Marcin Hoffmann. Vibration suppression with use of input shaping control in machining. *Sensors*, 22(6):2186, mar 2022.
- [15] Joonyoung Kim and Elizabeth A. Croft. Preshaping input trajectories of industrial robots for vibration suppression. *Robotics and Computer-Integrated Manufacturing*, 54:35–44, December 2018.
- [16] Wilson Linda S., Balestra Francis, Sangiorgi Enrico, Hayashi Yoshihiro, Takaura Norikatsu, Ishiuchi Hidemi, Gargini Paolo, and Conte Tom. International Roadmap for Devices and Systems (IRDS). Technical report, IEEE, 2023.
- [17] P.H. Meckl and P.B. Arestides. Optimized s-curve motion profiles for minimum residual vibration. In *Proceedings of the 1998 American Control Conference. ACC (IEEE Cat. No.98CH36207)*. IEEE, 1998.
- [18] Lucy Y. Pao and William E. Singhose. Robust minimum time control of flexible structures. *Automatica*, 34(2):229–236, feb 1998.
- [19] Markos Papageorgiou, Marion Leibold, and Martin Buss. *Optimierung - Statische, dynamische, stochastische Verfahren für die Anwendung*. Springer Berlin Heidelberg, Berlin, Heidelberg, 4., neu bearb. u. erg. aufl. 2015 edition, 2015.
- [20] U. H. Park, J. W. Lee, B. D. Lim, and Y. G. Sung. Design and Sensitivity Analysis of an Input Shaping Filter in the Z-Plane. *Journal of Sound and Vibration*, 243(1):157–171, May 2001.
- [21] Dan Pilbauer, Wim Michiels, Jaroslav Bušek, David Osta, and Tomáš Vyhlídal. Control design and experimental validation for flexible multi-body systems pre-compensated by inverse shapers. *Systems & Control Letters*, 113:93–100, March 2018.
- [22] Jinhua She, Lulu Wu, and Zhen-Tao Liu. Combining input shaping and adaptive model-following control for vibration suppression. *Journal of Advanced Computational Intelligence and Intelligent Informatics*, 25(1):56–63, January 2021.
- [23] Cristiana Silva and Emmanuel Trelat. Smooth regularization of bang-bang optimal control problems. *IEEE Transactions on Automatic Control*, 55(11):2488–2499, November 2010.
- [24] N. Singer, W. Singhose, and W. Seering. Comparison of filtering methods for reducing residual vibration. *European Journal of Control*, 5(2-4):208–218, jan 1999.
- [25] W. Singhose, W. Seering, and N. Singer. Residual vibration reduction using vector diagrams to generate shaped inputs. *Journal of Mechanical Design*, 116(2):654–659, June 1994.
- [26] W. E. Singhose, L. J. Porter, T. D. Tuttle, and N. C. Singer. Vibration reduction using multi-hump input shapers. *Journal of Dynamic Systems, Measurement, and Control*, 119(2):320–326, jun 1997.
- [27] W.E. Singhose, W.P. Seering, and N.C. Singer. Shaping inputs to reduce vibration: a vector diagram approach. In *Proceedings., IEEE International Conference on Robotics and Automation*. IEEE Comput. Soc. Press, 1990.
- [28] W.E. Singhose, Neil Singer, Convolv Inc, and Warren Seering. Design and implementation of time-optimal negative input shapers. March 1996.
- [29] William Singhose. Command Shaping for Flexible Systems: A Review of the First 50 Years. *International Journal Of Precision Engineering And Manufacturing*, 2009.
- [30] Khalid L. Sorensen, Aayush Daftari, William E. Singhose, and Keith Hekman. Negative input shaping: Eliminating overcurrenting and maximizing the command space. *Journal of Dynamic Systems, Measurement, and Control*, 130(6), oct 2008.
- [31] T. H. Tsang, D. M. Himmelblau, and T. F. Edgar. Optimal control via collocation and non-linear programming. *International Journal of Control*, 21(5):763–768, May 1975.
- [32] Joshua Vaughan, Aika Yano, and William Singhose. Comparison of robust input shapers. *Journal of Sound and Vibration*, 315(4-5):797–815, sep 2008.